Journal of the Iranian Chemical Society
https://doi.org/10.1007/s13738-020-01888-0

ORIGINAL PAPER

Friedel–Crafts benzylation of toluene catalyzed by $ZnCl_2/SiO_2$ heterogeneous catalyst to *para*- and *ortho*-mono-benzylated toluene

Anwar Iqbal[1,3] · Kok-Hou Tan[1] · U. S. Shaari[1] · N. I. N. B. Ahmad[1] · Farook Adam[1] · Hwei Voon Lee[2] · Rahimi M. Yusop[3] · N. H. H. Abu Bakar[1] · Hooi Ling Lee[4] · Hariy Pauzi[5] · Muhammad Fadhirul Izwan Abd Malik[5] · Ahmad Fadly Jusoh[6] · Lee D. Wilson[7] · M. N. Ahmad[8] · M. Hazwan Hussain[1] · Mohamad Nasir Mohamad Ibrahim[1]

Received: 28 May 2019 / Accepted: 17 February 2020

Abstract
A series of catalysts was prepared for the liquid-phase Friedel–Crafts benzylation of toluene with benzyl chloride (BC) by impregnating rice husk ash silica with $ZnCl_2$ (3 wt%, 6 wt%, 9 wt%, and 12 wt%) via a wet impregnation method. The XRD analysis indicates that the catalysts were amorphous with ill-defined pore systems. The XPS analysis detected the coexistence of ZnO nanoparticles together with $ZnCl_2$ on the catalyst surface, whereas the ^{29}Si NMR analysis indicates the formation of Si–O–Zn bond. Quantitative conversion of benzyl chloride (100%) was achieved within 3 h at 353 K when a catalyst with 9 wt% $ZnCl_2$ was used due to its narrow pore size and high surface area (635 $m^2\ g^{-1}$). *Para*- and *ortho*-mono-benzylated toluene was obtained as the products. The reaction is proposed to take place via weak attraction between benzyl chloride and the Zn through its chlorine atom. The catalyst was recycled four times with minimum loss (8%) in activity. The benzylation of benzene, toluene, *p*-xylene, and anisole followed the classical mechanism of Friedel–Craft-type acid-catalyzed benzylation reaction. The BC conversion increased in the order of toluene = *p*-xylene > anisole > benzene. The catalyst was also screened to be active in the benzoylation of toluene with benzoyl chloride (BOC). The conversion of BOC was 45% with selectivity toward 2-methylbenzophenone (50%) and 3-methylbenzophenone (50%).

Keywords Rice husk · Rice husk ash silica · Friedel–Crafts benzylation · $ZnCl_2$ · *Para*- and *ortho*-mono-benzylated toluene

Introduction

Friedel–Crafts reactions are widely used for the synthesis of substituted aromatic compounds [1]. In this reaction, the C–H bond will be converted to the C–C bond in the presence of a catalyst. Benzylation of toluene, benzene, and xylene that utilize alkylating agents such as benzyl chloride (BC) or benzyl alcohol (BOH) is among the types of Friedel–Crafts reactions used to produce important products such as mono-benzylated toluene (MBT), benzyltoluene, benzoic acid, and substituted diphenyl methane. These products, especially MBT, are a valuable commodity in pharmaceuticals and fragrance industries. Such compounds are also being used

✉ Anwar Iqbal
anwariqbal@usm.my

1 School of Chemical Sciences, Universiti Sains Malaysia, 11800 Minden, Penang, Malaysia

2 Nanotechnology and Catalysis Research Centre (NANOCAT), Institute of Postgraduate Studies, Universiti Malaya, 50603 Kuala Lumpur, Malaysia

3 School of Chemical Sciences and Food Technology, Faculty of Science and Technology, Universiti Kebangsaan Malaysia, 43600 UKM Bangi, Malaysia

4 Nanomaterials Research Group, Universiti Sains Malaysia, 11800 Minden, Penang, Malaysia

5 Science and Engineering Research Centre (SERC), Universiti Sains Malaysia, Engineering Campus, 4300 Nibong Tebal, Seberang Perai Selatan, Penang, Malaysia

6 Centre for Global Archaeological Research, Universiti Sains Malaysia, 11800 Minden, Penang, Malaysia

7 Department of Chemistry, University of Saskatchewan, 110 Science Place, Room 156 Thorvaldson Building, Saskatoon S7N 5C9, Canada

8 Experimental and Theoretical Research Lab, Department of Chemistry, Kulliyyah of Science, International Islamic University Malaysia, Bandar Indera Mahkota, 25200 Kuantan, Pahang, Malaysia

Published online: 27 February 2020

as monomers for polycarbonate resins, heat-transfer fluids, aromatic solvents, and fine chemicals [2–6].

Traditionally, strong Lewis and mineral acid catalysts such as $ZnCl_2$, $AlCl_3$, $FeCl_3$, HF, H_2SO_4, $TiCl_4$, and BF_3 were employed as homogeneous catalysts in this electrophilic substitution reaction [1, 3, 7]. Although these catalysts are very active, they are difficult to recycle. Besides, the reaction requires an over-stoichiometric amount of catalysts that generate toxic and corrosive waste [8, 9]. Heterogenization of the active sites on the surface of a solid can solve these problems. The heterogeneous catalytic system has several advantages over the homogeneous catalytic system, as follows: (1) The solid catalyst can be separated easily from the reaction mixture through filtration, (2) it produces a higher yield of products, (3) it requires only very small quantities of the catalyst, and (4) it can be recycled many times.

The surface of silica (SiO_2) consists of an abundant amount of silanol (Si–OH) groups which can form bonds with Lewis acids via a condensation reaction. Lewis acids supported onto silica have shown remarkable catalytic activity in various types of Friedel–Crafts reactions. He et al. [10] explored the catalytic activity of $AlCl_3$ immobilized on ordered (SBA-15 and MCM-41) and disordered silica (SiO_2 and SiO_2-Gel) for the Friedel–Crafts alkylation of benzene with a linear chain olefin, with 1-dodecene as the alkylating agent. Their findings indicate that the pore channel structure strongly influences the catalytic activity of the catalysts. The total conversion of 1-dodecene was achieved when $AlCl_3$ immobilized on SBA-15 was used with 50% product selectivity of 2-linear alkylbenzene. A series of thallium-containing mesoporous silica with different Tl contents was prepared by Baradji et al. [11] for the benzylation of benzene by benzyl chloride. Diphenylmethane was obtained as the sole product when a stoichiometric ratio of benzene and benzyl chloride was employed. The catalytic activity was attributed to the well-dispersed and stabilized thallium oxide particles on the silica support. Zup et al. [12] utilized silica-gel bound aluminum chloride (Si-$AlCl_x$) for Friedel–Crafts alkylation for a range of aromatics with alkyl halides under microwave irradiation. The catalysts were found to be much more reactive compared to a commercial $AlCl_3$ salt.

Since the discovery of MCM-41 in 1992, various types of silica with pore channel structures ranging from micropores to macropores have been synthesized and used as a support for a variety of catalysts. The silica precursor used in the synthesis of most siliceous materials such as tetraethyl orthosilicate (TEOS), tetramethyl orthosilicate (TMOS), and sodium silicate is of synthetic origin and very costly. Rice husk ash (RHA) offers a sustainable and greener source of silica. Amorphous silica can be obtained by pyrolyzing rice husk (RH) in a controlled environment at a temperature of around 500–600 °C. In previous studies, Al, Ga, In, and Fe were immobilized successfully within the matrix of silica from RH and RHA and used in the Friedel–Crafts reactions involving various types of aromatic compounds. For the Friedel–Crafts benzylation of toluene, Fe- and 4-(methylamino)benzoic acid-incorporated silica from RH improved the formation of mono-benzylated toluene to almost 99%. The nitrogen atom from the benzoic acid formed dative bonds with the carbocation fixing them at the active sites enabling better interaction with the toluene to form more mono-benzylated toluene compared to di-benzylated toluene [13].

Rice husk ash-supported indium was synthesized for the benzylation of benzene and substituted benzenes. The In^{3+} ions were found to be homogeneously distributed on the surface of the catalyst. The total conversion of benzene was achieved with ca. 90% selectivity toward diphenylmethane (DPM). The reactivity trend was shown to be as follows: benzene > toluene > ethyl benzene > anisole, where this trend was opposite to the classical acid-catalyzed Friedel–Crafts-type benzylation reaction [14]. The silica was also used as a support for Al^{3+} and Ga^{3+} ions. Similar to the Fe^{3+} ion, the Al^{3+} and Ga^{3+} ions were homogeneously distributed. The selectivity of DPM when the catalysts were used was ~ 80–86% with 100% BC conversion [15], where the silica supports used contain mesopores.

In the present study, we explored the potential of $ZnCl_2$ incorporated on silica from rice husk ash ($ZnCl_2/SiO_2$) catalysts for the Friedel–Crafts benzylation of toluene with BC as the benzylation agent. Zinc chloride ($ZnCl_2$) is widely available and moderately active compared to other Lewis acids. The use of $ZnCl_2$ as a catalyst for Friedel–Crafts reactions can be traced back to 1989. In that year, $ZnCl_2$ supported on montmorillonite, K10, was reported and subsequently commercialized under the trade name Clayzinc for the benzylation of benzene and other aromatic compounds [16, 17]. The combined analysis of FTIR, XRD, ^{29}Si NMR, and XPS was used to elucidate the surface structure of the active catalyst. Experimental parameters such as reaction time, surface texture, reaction temperature, mass of catalyst, and the molar ratio of toluene:BC were systematically studied. A detailed mechanism of the reaction which includes the surface-active sites of the catalyst was proposed as well. To the best of our knowledge, the physicochemical and catalytic properties of $ZnCl_2/SiO_2$ catalysts have not been reported. The catalyst is appealing on the industrial viewpoint since the materials used are considered cheap and widely available.

Materials and methods

Materials

The rice husk was obtained from a rice mill in Penang, Malaysia. Other reagents such as nitric acid (Qrëc 65%),

toluene (Qrëc 99.5%), benzyl chloride (SAFC 97%), benzyl alcohol (Acros 99.5%), benzoyl chloride (Fluka 99%), benzene (Merck 99.7%), anisole (Fluka 99%), *p*-xylene (Sigma 99%), acetone (Sigma-Aldrich ≥ 99.5%), ethanol (Sigma-Aldrich ≥ 99.8%), sodium hydroxide pellets (R&M Chemicals 99%), and CTAB (Riedel–de Haen 98%) were of analytical grade and were used as received without further purification.

Methods

Preparation of RHA

The preparation of RHA was carried out based on the method reported by Adam et al. [18]. Tap water was used to clean the RH to remove dirt and dried at room temperature for 24 h. The clean RH (30 g) was stirred in 750 ml of 1.0 M HNO_3 at room temperature for 24 h. Distilled water was used to wash the RH until the pH of the filtrate remained constant (pH 5). The treated RH was dried at 100 °C in an oven for 24 h followed by pyrolysis in a muffle furnace at 600 °C for 6 h to obtain white RHA.

Preparation of silica support

The silica from RHA was prepared according to the reported method by Iqbal et al. [19]. In a 500 mL Nalgene bottle, 100 mL of 0.8 M NaOH solution was mixed with 3.2 g of RHA. The mixture was stirred at 80 °C under constant stirring for 1 h. The resulted sodium silicate was then filtered to remove undissolved RHA. A CTAB solution was prepared by dissolving 2.9 g of CTAB in 50 mL of distilled water at room temperature. This CTAB solution was added to the clear sodium silicate while constantly stirring at 80 °C. The pH of the mixture was reduced to pH 10 by adding 2.0 M HNO_3. A white gel started to form at pH 10. The gel was aged in the mother liquor under constant stirring at 80 °C for 57 h, followed by centrifugation and filtration. The gel was finally rinsed with distilled water and acetone. The recovered xerogel was dried in the oven for 24 h at 100 °C. The xerogel was ground into a fine powder and calcined in a muffle furnace for 6 h at 600 °C to remove the CTAB. The xerogel was labeled as RHA-SiO_2.

Impregnation of $ZnCl_2$ on the surface of silica

In a typical procedure, the $ZnCl_2$ salt (based on silica weight) was dissolved in a beaker containing 20 mL of ethanol. Into this solution, 1.0 g of RHA-SiO_2 was added and vigorously stirred at 50 °C in a water bath until all the solvent evaporated. The resulting powder was dried in an oven at 110 °C before calcination at 200 °C for 2 h. The catalysts were labeled as RHA-*x* (*x* = 3, 6, 9, and 12) depending on the wt% of $ZnCl_2$.

Catalyst Characterizations

The prepared samples were characterized by FTIR (PerkinElmer System 2000) spectroscopy, N_2 adsorption–desorption porosimetry (Micromeritics Instrument Corporation model ASAP 2000, Norcross), powder X-ray diffractometry (Siemens Diffractometer D5000, Kristalloflex), scanning electron microscopy (SEM, Leica Cambridge S360), energy-dispersive spectrometry (EDAX FALCON SYSTEM), and transmission electron microscopy (TEM, Philips CM12 Instruments). The solid-state ^{29}Si MAS NMR spectra were obtained on a Bruker DSX-3000. Chemical shifts were referenced to tetramethylsilane (TMS). The XPS wide and narrow scan spectra were acquired using AXIS Ultra DLD, Kratos, equipped with an Al Kα X-ray source (1486.6 eV) at 10 mA, 15 kV, using the multichannel plate and delay line detector (DLD). The analysis was performed in the hybrid lens mode with the slot aperture, and the analyzer was operated in fixed analyzer transmission (FAT) mode with pass energy of the hemispherical analyzer set at 160 eV for the survey/wide scan and 20 eV for the high-resolution scans/narrow scans, while the minimum number of scanning was ten times. The spectra were analyzed using vision software (Kratos, UK), which included vision manager and vision processing. The linear method was used for background subtraction and curve fitting. The binding energy was referenced to an adventitious carbon at 284.6 eV.

The acidity of the catalysts was studied using temperature-programmed desorption (TPD-NH_3) with NH_3 as a probe molecule. The analysis was carried out using TPD/R/O 1100 (Thermo Finnigan) instrument equipped with a thermal conductivity detector (TCD). The catalyst (~0.05 g) was pretreated by N_2 gas flow for 30 min at 250 °C, followed with NH_3 gas for an hour at ambient temperature to allow adsorption of NH_3 onto the surface. The excess NH_3 was subsequently flushed with the N_2 gas flow at a rate of 20 cm^3/min. The desorption of NH_3 from the acid sites of the catalyst was detected by TCD under helium gas flow (30 mL/min) from 50 to 900 °C and held for 30 min [20]. The bulk Zn content was determined using inductively coupled plasma-optical emission spectrometry (ICP-OES) (PerkinElmer, ELAN 6100).

Catalytic activity

In a typical liquid-phase Friedel–Craft benzylation reaction, a mixture of toluene (15.0 mL, 140 mmol) and benzyl chloride (1.0 mL, 9 mmol) was taken in a 50.0-mL round-bottom flask fitted with a reflux condenser. The reaction mixture was stirred well in a preheated oil bath at 353 K before adding

the catalyst. The reaction is considered to begin when the catalyst was added to the flask. The reaction medium was stirred for 6 h. Samples (0.5 mL) were withdrawn at regular intervals and analyzed with gas chromatography (GC), model Clarus 500 PerkinElmer setup with an Elite 5 capillary column (PerkinElmer), and a flame ionization detector (FID). About 0.2 µL of the sample was injected into the GC–FID for analysis. The temperature program for the GC analysis was as follows: initial temperature: 90 °C; initial time: 0 min; Ramp 1:4 °C/min; Temp 2: 175 °C/min; final temperature: 250 °C. Gas chromatography–mass spectrometry (GC–MS), model Clarus 600 PerkinElmer, was used to confirm the products. Conditions used for GC–MS analysis were similar to the GC. For the hot filtration test, the catalyst was removed at 10 min and the reaction was continued using the filtrate. For the reusability test, the catalyst was separated by hot filtration followed by washing with hot solvent and then dried at 373 K before reusing.

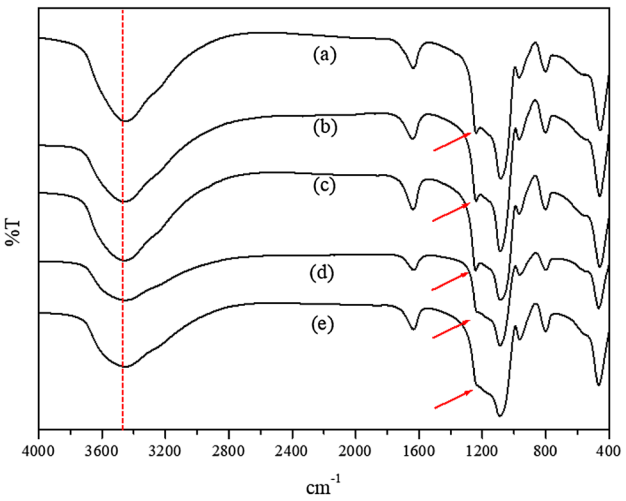

Fig. 1 The FTIR spectra of (a) RHA-SiO_2, (b) RHA-3, (c) RHA-6, (d) RHA-9, and (e) RHA-12. The disappearance of IR band attributed to ν_{as} (Si–O–Si) at 1224 cm^{-1} is indicated by the red arrows

Results and discussion

Catalyst characterization

The ICP-OES analysis indicates that the total concentration of Zn increased as the wt% was increased. From the XPS analysis, the maximum concentration of Zn that can be supported on the support is ~ 1.0 wt%. The concentration of elements detected on the surface of the catalysts by XPS is given in Table 1 together with the total Zn concentration detected by ICP-OES.

The FTIR spectra of the catalysts are shown in Fig. 1. The broad band at ~ 3400 cm^{-1} (shown by the red dotted line) is associated with the –OH bond stretching vibration of the surface silanol groups and hydrogen-bonded adsorbed water molecules. The bands at 1224 and 1085 cm^{-1} are attributed to ν_{as}(Si–O–Si). The intensity of the band at 1224 cm^{-1} (shown by red arrows) progressively reduced as the $ZnCl_2$ wt% was increased. The reduction in the band intensity suggests that the surface Si–OH undergone structural change leads to the formation of Si–O–Zn bonds. A group of bands at 961, 804, and 457 cm^{-1} are assigned to ν_{as}(Si–OH), ν_s(Si–O–Si), and Si–O–Si, respectively. The bending mode of adsorbed water molecules is indicated by the appearance of the band at 1635 cm^{-1} [21, 22].

Table 1 The elements detected on the surface of the catalysts by XPS analysis

Catalyst	XPS analysis (wt%)				ICP-OES (ppm)
	Si	Zn	Cl	O	Zn
RHA-3	20.66	0.38	0.17	58.66	147
RHA-6	26.94	1.05	0.23	63.42	347
RHA-9	28.03	1.06	0.26	66.43	607
RHA-12	27.28	1.08	0.34	63.96	885

Figure 2a represents the low-angle X-ray diffraction (LAXD) diffractograms of the catalysts. From Fig. 2a, three signatures are noted in the diffractogram of RHA-SiO_2 at $2\theta = 2.5°$, 4.32°, and 4.98°. These reflections correspond to the (1 0 0), (1 1 0), and (2 0 0) planes, respectively. The weak intensity of this peak indicates that RHA-SiO_2 has poor crystallinity and ill-defined hexagonal pore geometry [23]. In comparison with RHA-SiO_2, the reflection line of (1 0 0) plane shifted to $2\theta = 2.7°$ when 3 wt% and 6 wt% of $ZnCl_2$ was impregnated. Increasing the $ZnCl_2$ content to 9 wt% and 12 wt% diminished all the reflection lines. The absence of notable scattering in the diffractograms of RHA-9 and RHA-12 indicates the presence of a highly disordered pore system. The d-spacing (d_{100}) values of RHA-SiO_2, RHA-9, and RHA-12 were 1.77, 1.63, and 1.63 nm, respectively, whereas the unit cell parameters (a_0) were 2.04, 1.88, and 1.88 nm, respectively. The decrease in the d_{100} and a_0 indicates the loss of structural regularity and pore-size narrowing [24]. The d_{100} was calculated from the XRD pattern by Bragg's equation ($2d \sin\theta = \lambda$, where $\lambda = 1.5406$ Å for the Cu Kα line), whereas the a_0 was determined using the formula $a_0 = 2d_{100}/\sqrt{3}$. The wide-angle X-ray diffraction (WAXD) pattern of the catalysts is shown in Fig. 2b. The broad band centered at $2\theta = 23°$ is due to the presence of amorphous silica [25]. The absence of reflection lines related to the ZnO indicates that the concentration of ZnO particles might be too low for detection [26] or the ZnO nanoparticles exist in a highly amorphous state [27].

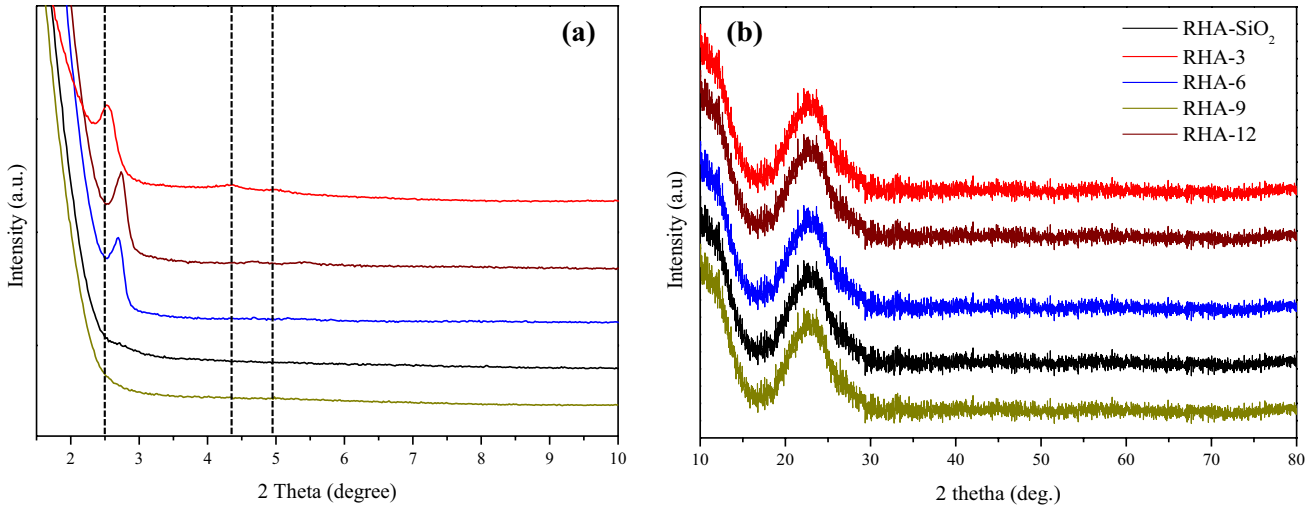

Fig. 2 The **a** LAXD and **b** WAXD diffractograms of RHA-3, RHA-6, RHA-9, and RHA-12

The TEM micrographs of the catalysts are shown in Fig. 3. The pores in RHA-SiO_2 can be seen to be arranged in parallel and spirally order with stacked layers of silica sheets (Fig. 3a). The pore arrangement progressively deteriorated as the wt% of $ZnCl_2$ was increased. The pore structure can still be clearly seen in the TEM micrographs of RHA-3 (Fig. 3a) and RHA-6 (Fig. 3b). The spiral architecture cannot be seen in the TEM micrographs of RHA-9 and RHA-12. The TEM results are in agreement with the XRD results. The pore deterioration is indicated by decreased d_{100} and a_0 values and the disappearance of the XRD signature at $2\theta = 2.7°$.

The extent of silica condensation in the catalysts can be observed from the ^{29}Si MAS NMR spectra in Fig. 4. The two strong signals related to the Q^3 (− 102 ppm) and Q^4 (− 112 ppm) and a weak signal related to Q^2 (− 93 ppm) are observable in the spectrum of RHA-SiO_2. The weak Q^2 signal corresponds to the geminal silanols, whereas the Q^3 and Q^4 signals are associated with the isolated silanols and siloxanes, respectively [28]. In the spectra of $ZnCl_2$ containing catalysts, only Q^3 and Q^4 signals can be observed. The disappearance of the Q^2 signal suggests the substitution of H atoms of the silanols by Zn atom to form Si–O–Zn bonds.

The TPD-NH_3 and acidity strength distribution are given in Fig. 5. The TPD pattern of the catalysts showed NH_3 desorption peak has T_{max} lower than 200 °C. This implies that the catalysts contain weak acid sites. The RHA-3 has the highest acid density (1089 µmol/g), whereas RHA-12 has the lowest density (229 µmol/g). The acid density of RHA-6 and RHA-9 was 495 and 635 µmol/g, respectively.

The N_2 adsorption–desorption isotherms of the catalysts are shown in Fig. 6. The uptake profiles of RHA-SiO_2, RHA-3, and RHA-6 resemble Type I and Type IV isotherms. The Type I isotherm is indicated by a high N_2 uptake observed at a very low relative pressure (P/P_o) due to the filling of micropores, whereas the Type IV isotherm is evidenced by the existence of a hysteresis loop near the relative pressure 0.8–1.0. The loop is associated with the condensation of N_2 in the interparticle pore domain space of the powder grains. The RHA-9 and RHA-12 show a Type IV isotherm which is typical of mesoporous materials. These catalysts also show a H4 hysteresis loop. According to the IUPAC, the H4 hysteresis loop is associated with materials having narrow slit pores [29].

The pore-size distribution of the catalysts was determined using the DFT model. For RHA-SiO_2, pores in the range of supermicropores (11–20 Å) were detected. The impregnation of $ZnCl_2$ resulted in larger pore diameter. The pore-size distribution of RHA-3 was 10–16 Å and 20–45 Å, whereas the pore-size distribution of RHA-6 was 10–19 Å and 43–55 Å. Increasing the $ZnCl_2$ content to 9 wt% and 12 wt% yielded a catalyst with a single narrow pore size, while the pore size of RHA-9 and RHA-12 was 31 Å. During the impregnation process, the Zn ions may have blocked the micropores and leaving the larger mesopores open. The incorporation of 3 wt% and 6 wt% of $ZnCl_2$ resulted in a decrease in the surface area (SA, 20–100 $m^2\ g^{-1}$) compared to the BET SA of RHA-SiO_2 (1016 $m^2\ g^{-1}$). A further increase to 9 wt% and 12 wt% is accompanied by a more significant SA decrease. The SA of RHA-9 and RHA-12 was 623 and 494 $m^2\ g^{-1}$, respectively. Aside from clogging/blocking the micropores, the deposition of $ZnCl_2$ or ZnO nanoparticles in the pores may result in SA reduction, as evidenced by the reduction in the BET surface area. The micropores SA of RHA-SiO_2, RHA-3, and RHA-6 was 899, 842, and 814 $m^2\ g^{-1}$, respectively, where the textural parameters are summarized in Table 2.

The XPS spectra of all the catalysts were similar, and the representative spectra are shown in Fig. 7. The XPS

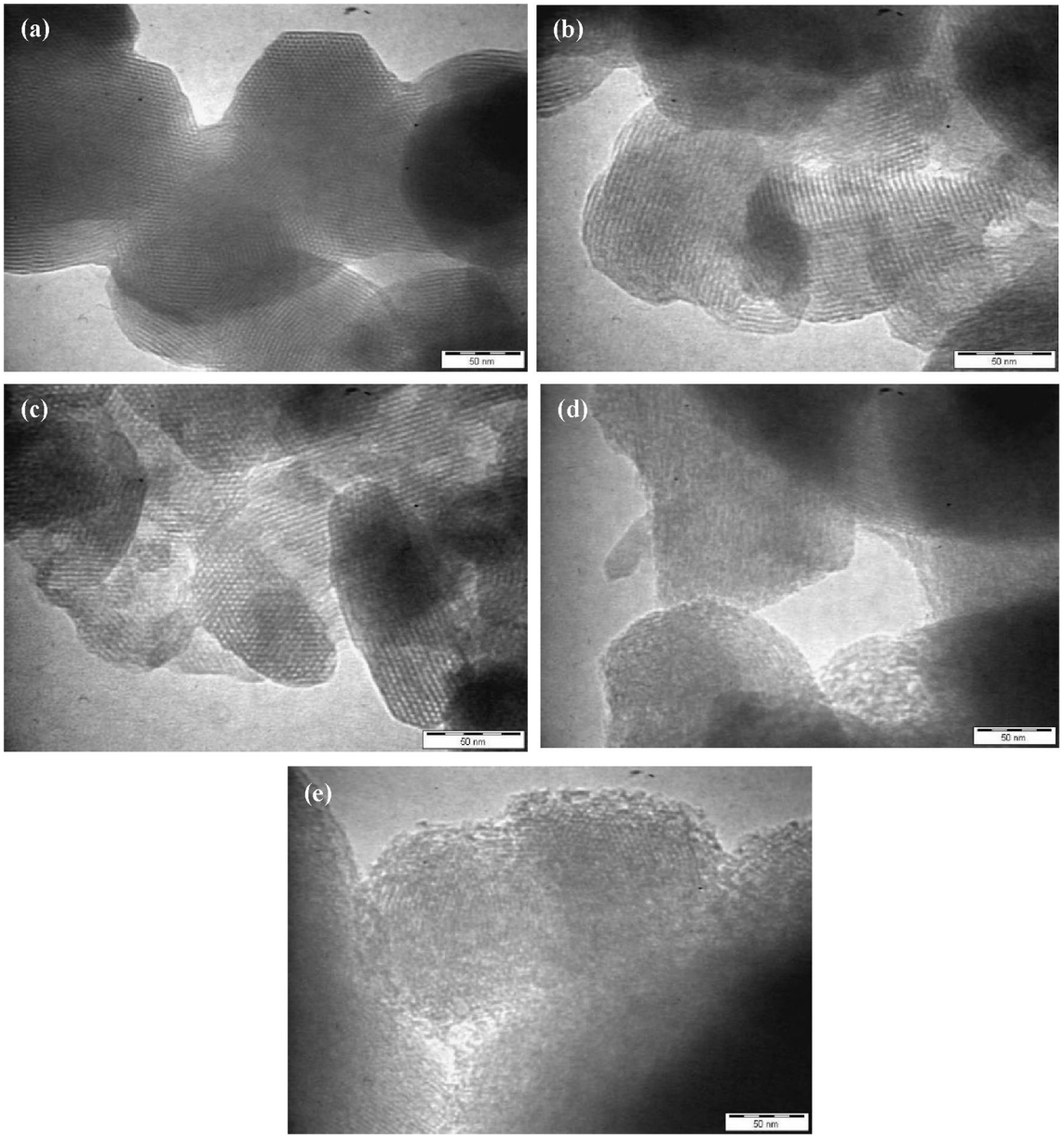

Fig. 3 The TEM micrographs of **a** RHA-SiO_2, **b** RHA-3, **c** RHA-6, **d** RHA-9, and **e** RHA-12

spectrum of Zn 2*p* (Fig. 7a) suggests the presence of two different types of Zn species. The presence of $ZnCl_2$ species is indicated by a doublet at 1023.2 and 1044.0 eV corresponding to the Zn $2p_{3/2}$ and Zn $2p_{1/2}$ lines, respectively [30, 31]. Another band at 1017.0 eV is a characteristic of ZnO [32]. The existence of this band indicates that a small amount of the $ZnCl_2$ was converted to ZnO during heat treatment. Compared to the XRD, XPS is more sensitive and able to detect finer particles of ZnO at lower concentrations.

The chlorine spectrum indicates the presence of Cl $2p_{1/2}$ and Cl $2p_{3/2}$ at 199.0 and 201.7 eV, respectively [33]. Only the signal related to the Si–O–Si was detected at 532.8 eV when the O 1*s* peak of the catalysts was deconvoluted. Signals related to the surface silanol groups (Si–OH) which generally appear at 534 eV were not observed. The absence of this signal strongly suggests the complete condensation of silanol groups to siloxane and the formation of Si–O–Zn species. The O 1*s* result is in agreement with the ^{29}Si NMR results which did not reveal signal related to surface Si–OH for the $ZnCl_2$ containing catalysts as well. However, silica itself is rich in oxygen. Thus, it can be difficult to resolve the types of oxygen bound to silica and zinc. Schmidt et al. [33] and Pillai et al. [34] reported the difficulty in resolving the signals of oxygen bound to zinc due to the excessive oxygen content in zeolite and alumina. They concluded that the surface hydroxyl groups of

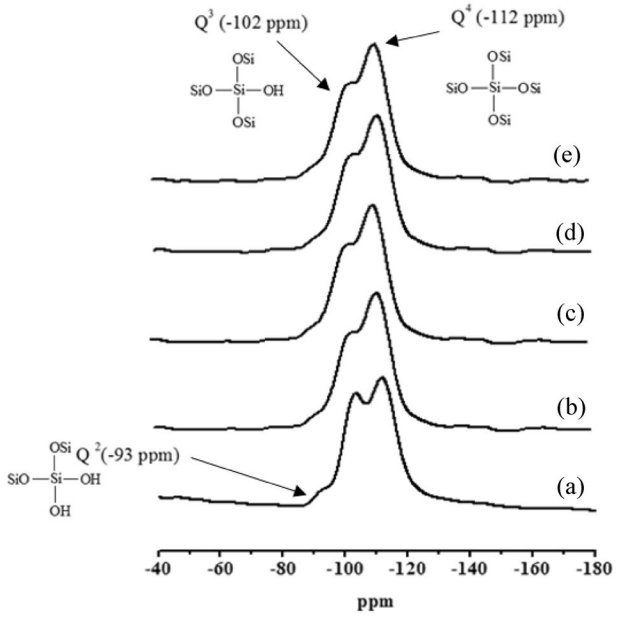

Fig. 4 The solid-state ^{29}Si NMR spectra of (a) RHA-SiO_2, (b) RHA-3, (c) RHA-6, (d) RHA-9, and (e) RHA-12

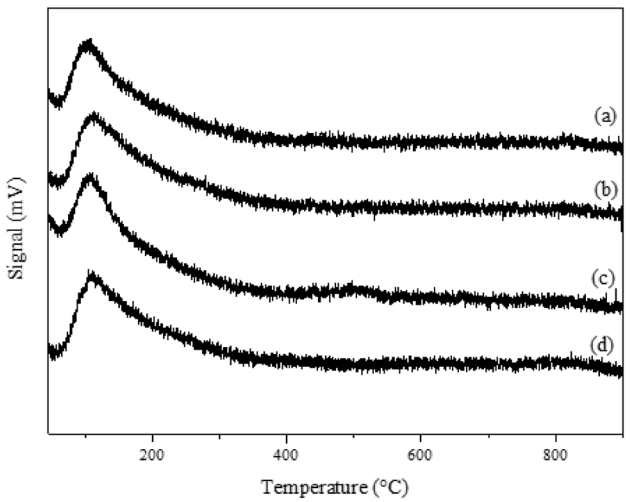

Fig. 5 The TPD-NH_3 analysis for catalysts: (a) RHA-3, (b) RHA-6, (c) RHA-9, and (d) RHA-12

the supports were eliminated during the modification with $ZnCl_2$ forming Al–O–Zn bonds. The existence of XPS signals related to Si 2*p* at 103.7 eV is due to the existence of Si^{4+} in the catalyst's framework [35].

Based on the results of ^{29}Si NMR and XPS analyses, the proposed surface structure of the catalyst is shown in Fig. 8. The ZnO nanoparticles are proposed to be deposited inside the pores, where the particles are held by the oxygen atoms from the silica framework.

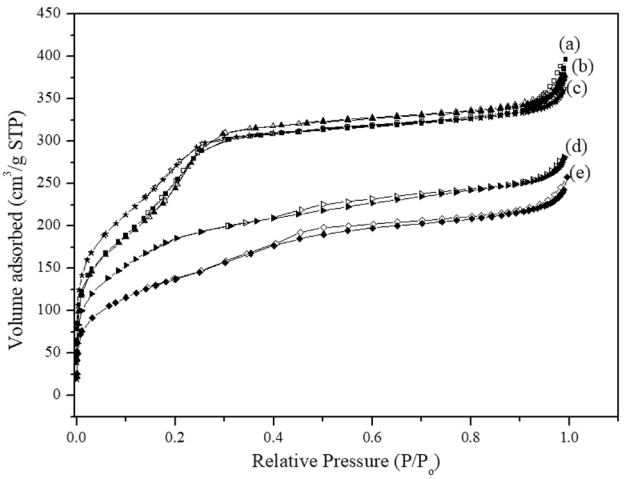

Fig. 6 The nitrogen adsorption–desorption isotherms of (a) RHA-SiO_2, (b) RHA-3, (c) RHA-6, (d) RHA-9, and (e) RHA-12

Table 2 Textural properties of RHA-SiO_2 and its modified forms (RHA-3, 6, 9, and 12) according to nitrogen adsorption isotherm results

Catalyst	BET surface area ($m^2\ g^{-1}$)	Micropore surface area ($m^2\ g^{-1}$)	Micropore volume ($cm^3 g^{-1}$)	DFT (Å)
RHA-SiO_2	1000	899	0.40	11–20
RHA-3	965	842	0.41	10–16 26–45
RHA-6	919	814	0.43	10–19 43–50
RHA-9	623	–	–	31
RHA-12	494	–	–	31

Friedel–Crafts Benzylation of Toluene

The influence of reaction time and types of benzylation agent in the Friedel–Crafts benzylation of toluene is shown in Fig. 9. The benzylation agents used were benzyl chloride (BC) and benzyl alcohol (BOH). Complete BC conversion was achieved within 3 h with 100% selectivity toward mono-benzylated toluene (*para*- and *ortho*-mono-benzylated toluene). The selectivity of *para*- and *ortho*-mono-benzylated toluene was 50% for each isomer, respectively. The conversion of styrene was ~ 30% when BOH was used as the benzylating agent. The water molecules produced from the benzylation reaction between toluene and BOH may have strongly adsorbed on the active sites of the catalyst surface thus preventing the reaction from taking place. The consecutive investigation was carried out using BC due to the higher conversion percentage. For comparison, the reaction was carried out using RHA-SiO_2 and $ZnCl_2$. The reaction did not occur when RHA-SiO_2 was used, whereas only ~ 60% of

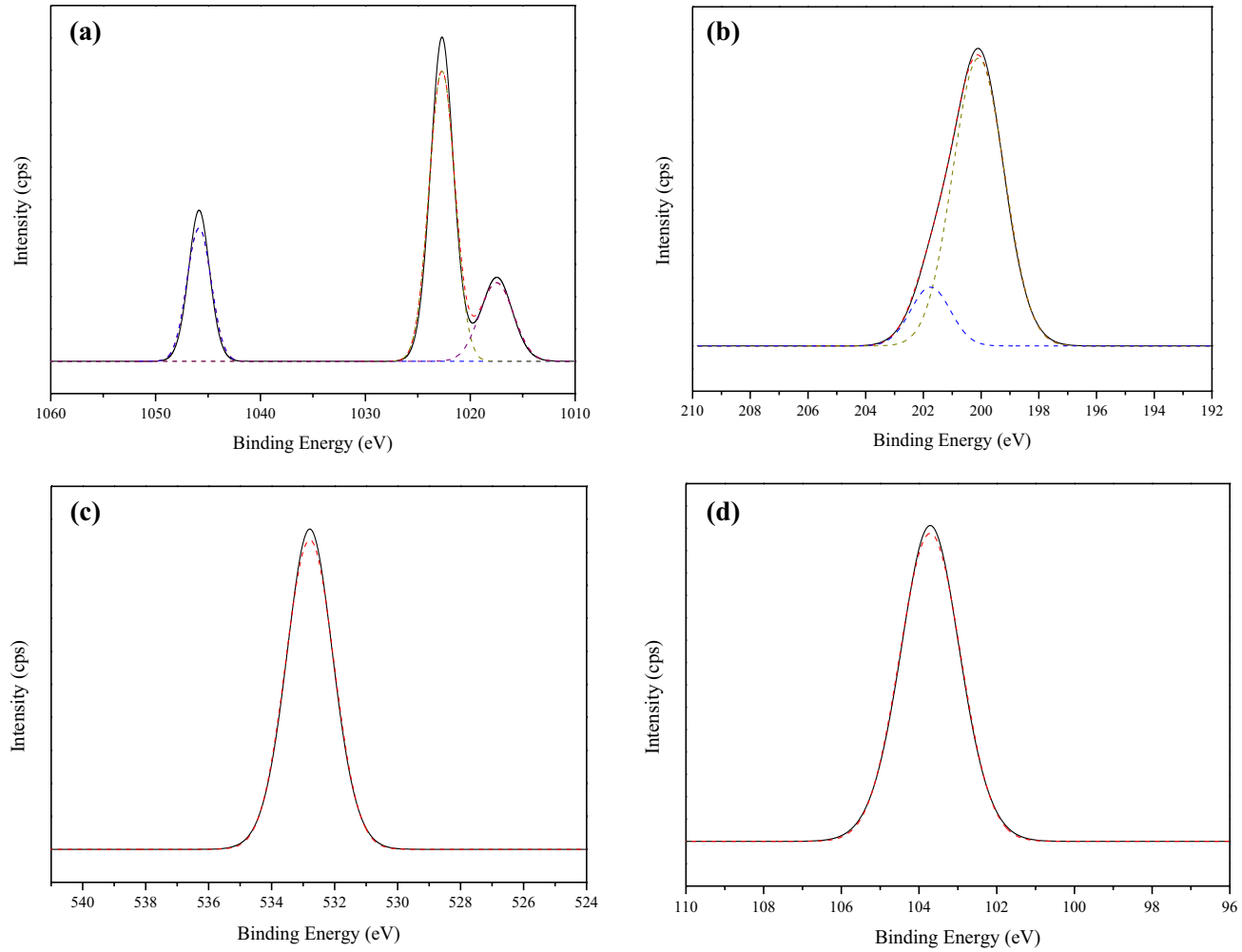

Fig. 7 The XPS spectra of **a** Zn 2*p*, **b** Cl 2*p*, **c** O 1*s*, and **d** Si 2*p* regions from the catalysts

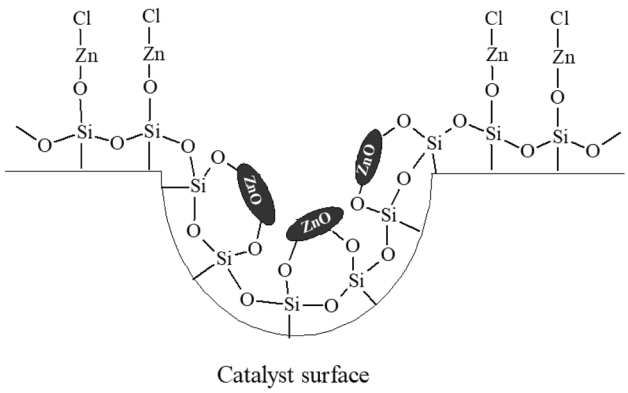

Fig. 8 The proposed surface structure of the catalyst

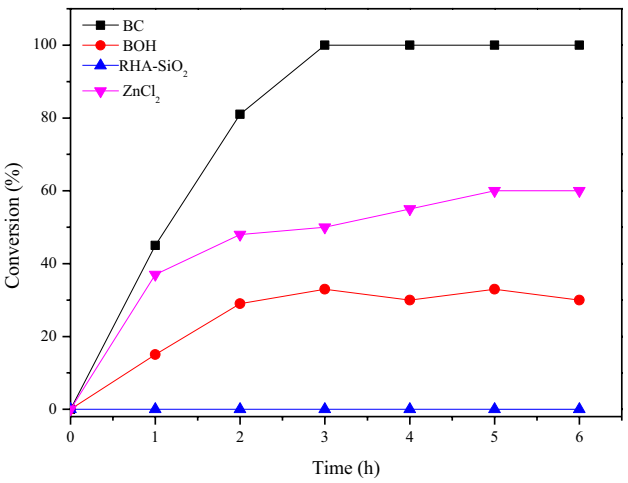

Fig. 9 The conversion of BC and BOH with respect to time. The reaction carried out using $ZnCl_2$ and RHA-SiO_2 was also included for the comparison. The reaction was carried out using 75 mg of catalyst at 353 K. The molar ratio of toluene:BC/BOH used was 15:1

toluene was converted in the presence of $ZnCl_2$. Even though $ZnCl_2$ is active, the metal salt cannot be easily separated and reused. The inactivity of RHA-SiO_2 is attributed to the very mildly acidic nature of silica.

The benzylation of toluene with BC was proposed to take place via electrophilic aromatic substitution. The reaction was initiated when the BC interacts on the surface of the catalyst to form a charged complex, **A** (Fig. 10). The interaction between Zn and the Cl atom of the BC is hypothesized to be weak. The interaction will also weaken the strength of the C–Cl bond of the BC [14].

The reaction between **A** and toluene, which is a weak nucleophile, formed a mixture of two intermediates: **B** and **B'**. The reorganization of electrons in the intermediates will form *para*- and *ortho*-mono-benzylated toluene and hydrochloric acid (HCl) as a by-product. The formation of *para*- and *ortho*-mono-benzylated toluene is shown in Fig. 11a, b, respectively. Based on the highest BC conversion rate when the reaction was carried out for 3 h, it was chosen as the optimum reaction time.

From the reaction profile shown in Fig. 12, the conversion of BC in the presence of RHA-3 (25%) and RHA-6 (43%) was lowest despite their larger BET SA. In the presence of micropores, the reactants had limited accessibility to the active sites, thus causing lower BC conversion. Besides that, a high concentration of product(s) may delay the desorption process of the products and possibly accumulate with the pore system [36]. These limitations may eventually lead to catalyst deactivation [37]. The conversion of BC increased to 100% when RHA-9 was used due to the presence of mesopores. It dropped to 62% when RHA-12 was used. This was due to its lower surface area compared to RHA-9.

The Friedel–Crafts benzylation reaction depends predominantly on the Lewis acidity of the catalysts. However, in this study, the trend of BC conversion was not in agreement with the acid density values obtained herein. Even though the acid density of the RHA-3 and RHA-6 was higher, the BC conversion was lower compared to RHA-9. Therefore, it can be concluded that acid density has moderate influence on the conversion of BC compared to the types of pores. Thus, RHA-9 was used as the best catalyst for the optimization of other parameters.

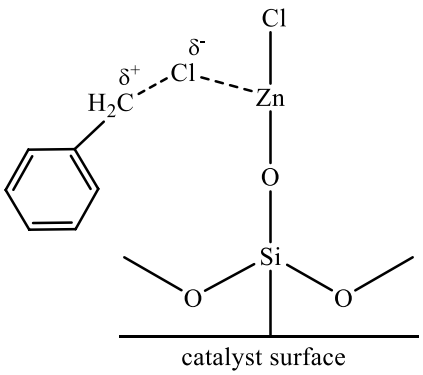

A

Fig. 10 The interaction of BC on the catalyst surface of the catalyst. The adsorption will form a weak interaction between the Cl and Zn atoms and weakens the C–Cl bond

The influence of the mass of RHA-9 on the conversion of BC is shown in Fig. 13. The catalyst weight was varied between 25 and 100 mg at 353 K with the reaction time set at 3 h, with 20:1 toluene:BC molar ratio. The BC conversion increased from 80 to 100% when the catalyst mass was increased from 25 to 50 mg due to the increase in the number of active sites. The further mass increase did not result in a significant change in BC conversion. The product distribution was not affected by the change in the catalyst mass. Based on the result, the optimum catalyst weight was 50 mg.

The influence of the molar ratio of toluene:BC on the conversion was investigated using 50 mg of RHA-9 for 3 h at the reflux temperature of 353 K. The mole ratio of toluene:BC studied was 10:1, 15:1, and 20:1, where the results are shown in Fig. 14. Increasing the molar ratio from 10:1 to 15:1 increased the conversion of BC from 60 to 85%. At the molar ratio of 20:1, the conversion reached 100%. The dilution of the reaction medium enabled BC to approach the active sites (Zn) for adsorption. The reaction conditions also prevented the reactants and products from being strongly adsorbed on the surface of the catalyst [38]. The optimum molar ratio of toluene:BC for this reaction was determined as 20:1.

In conclusion, to convert 100% BC to *para*- and *ortho*-mono-benzylated toluene, 50 mg of RHA-9 was required, where the reaction was carried out at 353 K with a molar ratio of toluene:BC, 20:1, for 3 h. The results for the recyclability of RHA-9 are shown in Fig. 15. The catalyst was used for four cycles (fresh and three reuses) without any significant loss. The BC conversion for the fresh and first reuse was 100%. The conversion of BC dropped by ca. 8% when the catalyst was reused for the second and third cycles. From these experimental results, RHA-9 is considered stable, where it must be noted that the selectivity toward the *mono*-benzylated toluene remained constant. Hence, the use of RHA-9 for the benzylation of toluene with BC has excellent potential for use in industrial applications. The hot filtration test (HFT) was conducted to determine the heterogeneity of the catalyst. After the removal of the catalyst, the conversion of toluene remained at 20%. The lower conversion of BC compared to RHA-9 further confirmed that the active sites did not leach from the support. If leaching had happened, the conversion rate will increase as the reaction progress. The reaction profile is shown in Fig. 16. The ICP-OES analysis did not detect any presence of Zn ion in the reaction mixture of the third cycle as well.

The benzylation reaction of different types of arenes was also investigated under the optimum conditions. The results are shown in Table 3. According to the classical mechanism of Friedel–Crafts-type acid-catalyzed benzylation reaction,

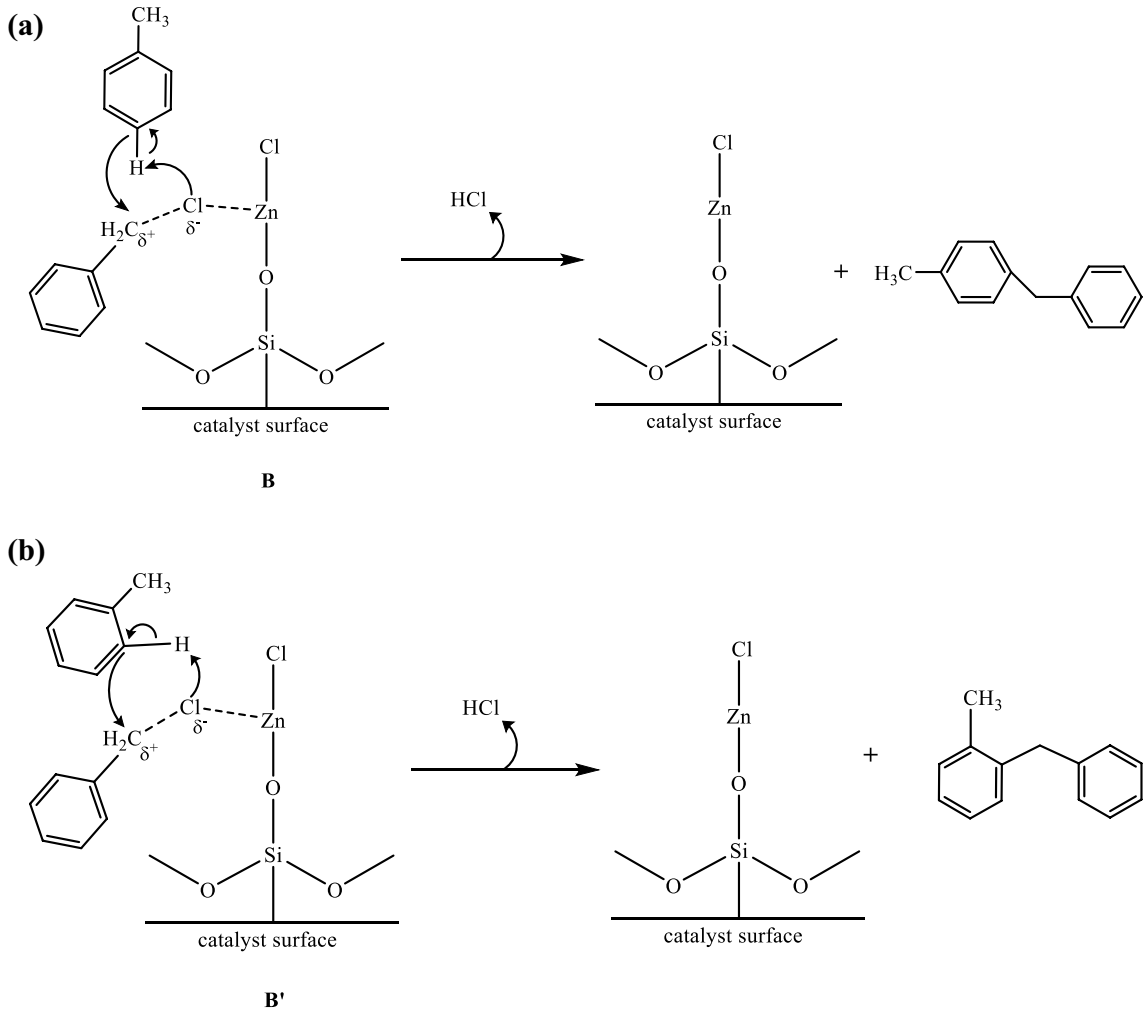

Fig. 11 The proposed mechanism for the Friedel–Crafts benzylation of toluene with benzyl chloride. The formation of *para*- and *ortho*-mono-benzylated toluene is shown in **a** and **b**, respectively

the reaction tends to proceed faster (easier) if one or more electron-donating groups are present in the aromatic ring [39]. From the table, the BC conversion increased in the order of toluene = *p*-xylene > anisole > benzene which is in accordance with the classical mechanism. Toluene contains a single electron-donating group (–CH_3), whereas *p*-xylene contains two. The presence of greater number of electron-donating groups increased the electrophilic substitution reaction. The methoxy (–OCH_3) group of anisole is electron withdrawing by the inductive effect of the oxygen atom which can reduce its reactivity toward electrophilic substitution reaction compared to toluene and *p*-xylene. Besides, the oxygen atoms can also form hydrogen bonds with the surface silanol group of the catalyst which may poison the catalyst [14]. Despite variation in the BC conversion, only mono-benzylated product was obtained.

The catalyst (RHA-9) was also screened for benzoylation of toluene with benzoyl chloride (BOC). The reaction was carried out under the optimum conditions determined for the benzylation of toluene. The conversion of BOC was 45% with selectivity toward 2-methylbenzophenone (50%) and 3-methylbenzophenone (50%). However, the conditions used for the screening may not be optimum. Thus, more in-depth investigations of various parameters are required.

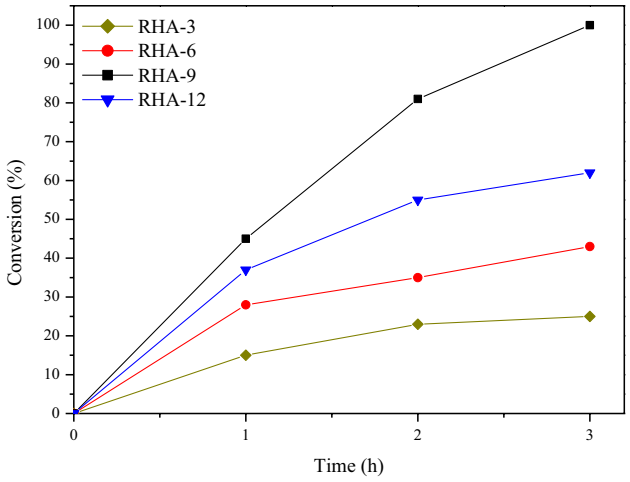

Fig. 12 The reaction profile expressed as conversion of BC versus time of the respective catalysts. The reaction was performed using 75 mg of catalyst at 353 K. The molar ratio of toluene:BC used was 20:1

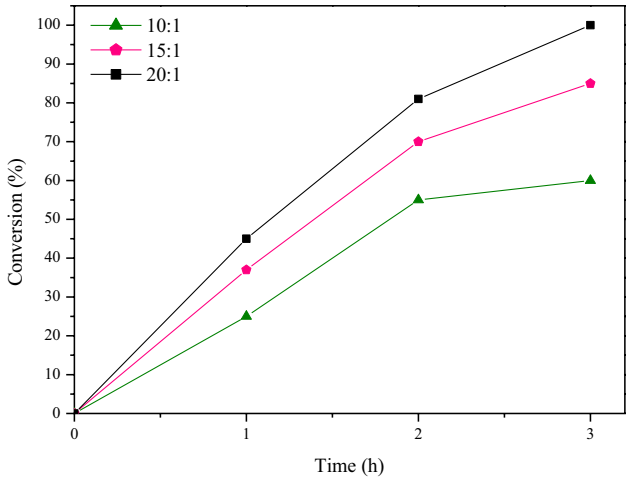

Fig. 14 The conversion of BC with respect to time for different molar ratios of toluene:BC. The reaction was carried out at 353 K using 50 mg of RHA-9

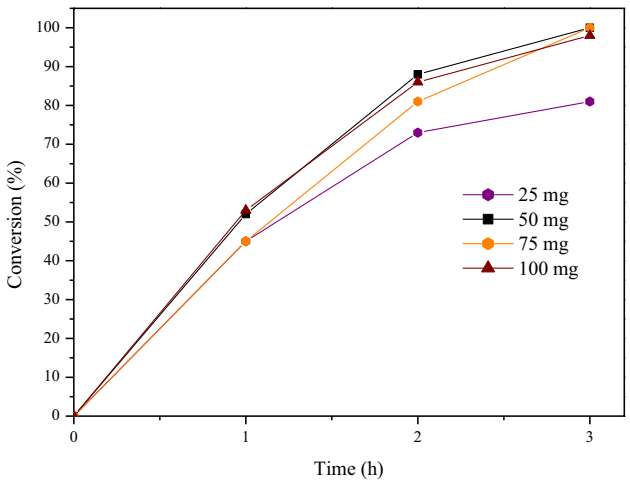

Fig. 13 The effect of different masses of RHA-9 on BC conversion. The reaction was carried out at 353 K. The molar ratio of toluene:BC used was 20:1

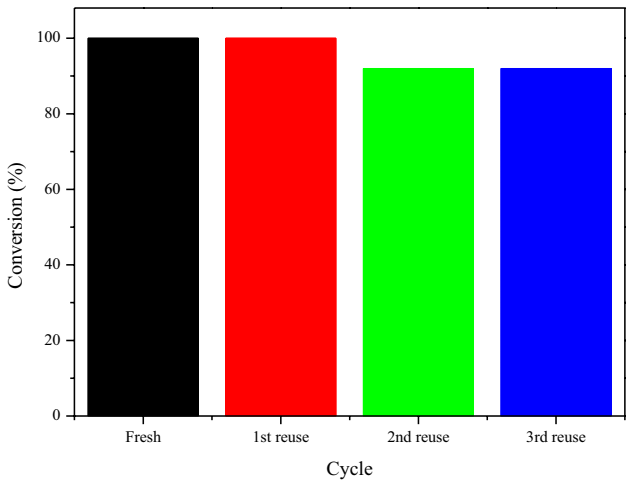

Fig. 15 The effect of recycling on the BC conversion at optimum conditions (RHA-9 mass: 50 mg, the molar ratio of toluene:BC: 20:1, reaction time: 3 h, and reaction temperature: 353 K)

Conclusion

The most catalytically active catalysts in the liquid-phase Friedel–Crafts benzylation of toluene with benzyl chloride (BC) were found to be RHA-9. The highest conversion (100%) of BC was achieved when 50 mg of catalyst was used together with the molar ratio of toluene:BC at 20:1. Under the optimum conditions, *para*- and *ortho*-monobenzylated toluene was formed with 50:50 selectivity. The catalytic activity of the catalyst was mainly influenced by the textural properties (pore system and surface area) rather than surface acidity. The electrophilic aromatic substitution reaction proceeded through the formation of a series of charged complexes. It was noted that the catalyst revealed minor leaching in the overall process. The reactivity trend for benzylation of different arenes was shown to adhere to the classical mechanism of Friedel–Crafts-type acid-catalyzed benzylation reaction; toluene = *p*-xylene > anisole > benzene.

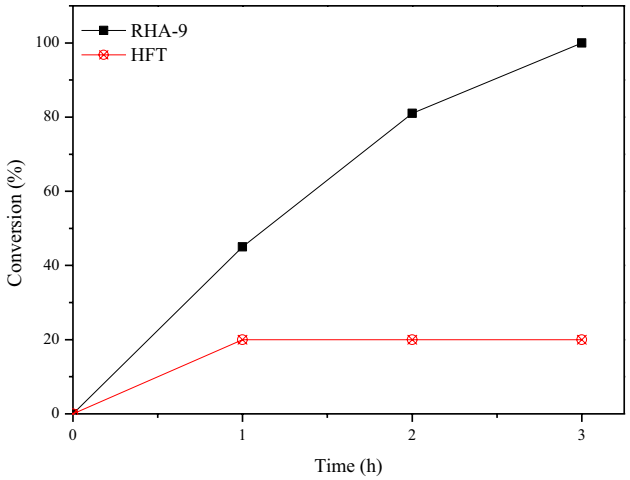

Fig. 16 Hot filtration test (HFT) indicates that after the catalyst was removed, the BC conversion remains constant at 20%. This observation indicates that the active sites did not leach from the support into the reaction medium. (RHA-9 mass: 50 mg, the molar ratio of toluene:BC: 20:1, reaction time: 3 h, and reaction temperature: 353 K)

Table 3 Benzylation of various arenes at 353 K with a molar ratio of arene:BC, 20:1, for 3 h

Arene	BC conversion (%)	Mono-benzylated (%)
Benzene	44	100
Anisole	64.3	100
Toluene	100	100
p-xylene	100	100

Acknowledgements We would like to thank the Malaysian Government,Universiti Sains Malaysia and Universiti Kebangsaan Malaysia for supporting this work through the Research University Grant (RUI) (1001/PKIMIA/8011083), Short Term Grant (304/PKIMIA/6313215) and Geran Universiti Penyelidikan Universiti Kebangsaan Malaysia (GUP-2019-045). We would like to extend our gratitude to the Ministry of Education, Malaysia (Higher Education) and Universiti Sains Malaysia for the Postdoctoral Training Fellowship awarded to Anwar Iqbal.

References

1. G.A. Olah, *Friedel–Crafts and Related Reactions* (Wiley, New York, 1964), p. 623
2. A.P. Singh, D. Bhattacharya, S. Sharma, J. Mol. Cat. A Chem. **102**, 139–145 (1995)
3. H. Jin, M.B. Ansari, E.Y. Jeong, S.E. Park, J. Catal. **291**, 55–62 (2012)
4. S.K. Jana, Catal. Surv. Asia **9**, 25–34 (2005)
5. A. Vinu, D.P. Sawanat, K. Ariga, M. Hartmann, S.B. Halligudi, Microporous Mesoporous Mater. **80**, 195–203 (2005)
6. V.V. Bokade, G.D. Yadav, J. Nat. Gas Chem. **16**, 186–192 (2007)
7. R.A. Sheldon, H. van Bekkum, Fine Chemicals through Heterogeneous Catalysis (Wiley: Weinheim, New York, 2008), p. 151
8. K. Shimizu, A. Satsuma, Energy Environ. Sci. **4**, 3140–3153 (2011)
9. M. Guisnet, M. Guidotti, Catalysts for Fine Chemical Synthesis: Microporous and Solid Catalysts (Wiley, Portugal, 2006) p. 40
10. Y. He, Q. Zhang, X. Zhan, D. Cheng, F. Chen, Chin. J. Chem. Eng. **25**, 1533–1538 (2017)
11. A. Baradji, K. Bachari, J. Amari, J. Chem. **10**, 179–183 (2017)
12. L.R. Zupp, V.L. Campanella, D.M. Rudzinski, F. Beland, R. Priefer, Tetrahedron Lett. **53**, 5343–5346 (2012)
13. F. Adam, J. Andas, J. Colloid Interface Sci. **311**, 135–143 (2007)
14. A.E. Ahmed, F. Adam, Microporous Mesoporous Mater. **103**, 284–295 (2007)
15. A.E. Ahmed, F. Adam, Microporous Mesoporous Mater. **118**, 35–43 (2009)
16. J.H. Clark, A.P. Kybett, D.J. Macquarrie, S.J. Barlow, P. London, J. Chem. Soc. Chem. Commun. **18**, 1353–1354 (1989)
17. J.H. Clark, S.R. Cullen, S.J. Barlow, T.W. Bastock, J. Chem. Soc. Perkin. Trans. **2**, 1117–11130 (1994)
18. F. Adam, J.N. Appaturi, R. Thankappan, M.A.M. Asri, Appl. Surf. Sci. **257**, 811–816 (2010)
19. A. Iqbal, T.K. Hou, U.S. Shaari, F. Adam, N.H.H. AbuBakar, L.D. Wilson, N.F. Jaafar, M. Hazwan Hussain, M.A. Afandi, Mater. Today Proc. **5**, 21584–21593 (2018)
20. N. Asikin-Mijan, H.V. Lee, G. Abdulkareem-Alsultan, A. Afandi, Y.H. Taufiq-Yap, J. Clean. Prod. **167**, 1048–1059 (2017)
21. G. Mohammadnezhad, S. Abad, R. Soltani, M. Dinari, Ultrason. Sonochem. **39**, 765–773 (2017)
22. F. Raji, M. Pakizeh, Appl. Surf. Sci. **282**, 415–424 (2013)
23. Y. Wang, X. Bai, F. Wang, H. Qin, C. Yin, S. Kang, X. Li, Y. Zuo, L. Cui, Sci. Rep. **6**, 1–7 (2016)
24. M. Selvaraj, A. Pandurangan, Ind. Eng. Chem. Res. **43**, 2399–2412 (2004)
25. R. Tayebee, M.M. Amini, M. Akbari, A. Aliakbari, Dalton Trans. **44**, 9596–9609 (2015)
26. D. Murzin, *Engineering Catalysis* (Hubert & Co. GmbH & Co. KG, Gottingen, 2013)
27. L.I. Ali, S.A. El-Molla, N.H. Amin, A.A. Ebrahim, H.R. Mahmoud, Arab. J. Chem. **9**, 1242–1251 (2016)
28. Y. Cabrera, A. Cabrera, F.H. Larsen, C. Felby, Holzforschung **70**, 709–718 (2016)
29. S. Lowell, J. E. Shields, M. A. Thomas, M. Thommes, Characterization of Porous Solids an Powders: Surface Area, Pore Size and Density (Kluwer Academic Publishers, The Netherlands, 2004), p. 44
30. C. D Wagner, The NIST Photoelectron Spectroscopy (XPS) Database (US Government Printing Office, Washington DC, 1991), p. 22
31. R.F. Mulligan, A.A. Iliadis, P.R. Kofinas, J. Appl. Polym. Sci. **89**, 1058–1061 (2003)
32. H.A. Ali, A.A. Iliadis, R.F. Mulligan, A.V.W. Cresce, P. Kofinas, U. Lee, Solid-State Electron. **46**, 1639–1642 (2002)
33. S.A. Schmidt, N. Kumar, A. Shchukarev, K. Eränen, J.-P. Mikkola, D.Y. Murzin, T. Salmi, Appl. Catal. A **468**, 120–134 (2013)
34. S.K. Pillai, S. Hamoudi, K. Belkacemi, Fuel **110**, 32–39 (2013)
35. L. Han, X.-G. Jiang, T.-L. Lu, B.-S. Wang, J. Xu, Y.-Z. Zhan, J.-F. Wang, A. Rawal, C. Zhao, Fuel Process. Technol. **162**, 87–89 (2017)
36. R. Aleixoa, R. Elvas-Leitão, F. Martins, A.P. Carvalho, A. Brigas, A. Martins, N. Nunes, Mol. Catal. **434**, 175–183 (2017)
37. A. Ramanathan, H. Zhu, R. Maheswari, B. Subramaniam, Chem. Eng. J. **278**, 113–121 (2015)
38. K.Y. Nandiwale, P. Thakur, V.V. Bokade, Appl. Petrochem. Res. **5**, 113–119 (2015)
39. V.R. Choudhary, S.K. Jana, J. Mol. Catal. A: Chem. **180**, 267–276 (2002)